R2-C.1: Thin Film Fluorescent Sensors for Explosives Detection

I. PARTICIPANTS

Faculty/Staff			
Name	**Title**	**Institution**	**Email**
William B. Euler	PI	URI	weuler@chm.uri.edu
Richard Sweetman	High School Teacher	Middletown High School	rsweetman@MPSRI.NET
Graduate, Undergraduate and REU Students			
Name	**Degree Pursued**	**Institution**	**Month/Year of Graduation**
Mona Alhasani	PhD	URI	12/2017
Mingyu Liu Chapman	PhD	URI	5/2018
Matthew Mullen	PhD	URI	5/2018
Elsa Ortega	PhD	URI	5/2018
Elizabeth Kohr	PhD	URI	5/2019

II. PROJECT DESCRIPTION

Core funding for this project ends in Year 3 per the outcome of the Biennial Review process. Currently funded students will be supported via the ALERT Science and Engineering Workforce Development Program (SEWDP) (formerly known as the ALERT Career Development Grant Program) so as to not impact their degrees. Results of the student work will be reported in a special section of the ALERT Year 4 Annual Report.

A. Project Overview

Detection of trace quantities of explosives in the gas phase is a pressing societal issue, of special importance to homeland security and a significant challenge to analytical chemistry. The low vapor pressure of most explosives, in the parts per billion (ppb) to parts per trillion (ppt) ranges at room temperature, pushes the limits for most methods. Modern fluorescent techniques are capable of detection in this range [1-3] and this has been adapted in a variety of ways for explosives detection for many years [4-33]. Improved methods for trace explosives detection is desirable, and studies to improve the sensitivity by enhancing the fluorescent signal or to improve selectivity by using arrays of fluorophores have been reported [18, 34-38], but all of these approaches require expensive or generally unavailable materials. Thus, our objective is to design sensors that can detect explosives in the gas phase at natural vapor pressures while using readily available components.

B. Biennial Review Results and Related Actions to Address

The project was cut after the Biennial Review. According to the major comments received from the reviewers, it was unclear how the sensor system would operate in a dirty environment with many other potential analytes present. The reviewers were also skeptical about a transition pathway. Tests of common interferants have begun to address the former point. Closer interactions with an industrial partner have also been initiated.

Through discussion following the Biennial Review process, ALERT requested and received authorization to use funding from the ALERT Science and Engineering Workforce Development Program (SEWDP) (formerly known as the ALERT Career Development Grant Program) to support graduate students who were working on cut projects such as this for up to two years in an effort to allow the students to graduate as planned. Elizabeth Kohr, Mingyu Liu, Matthew Mullen and Elsa Ortega, all PhD students working on this project are expected to be provided support for stipends during the summer of 2017.

C. State of the Art and Technical Approach

We had discovered that xanthene dyes interact with a variety of explosives and related molecules in dimethyl formamide (DMF) solution and these can be detected by changes in the emission. The xanthenes were chosen because they are readily available and inexpensive laser dyes with high quantum yields. Concurrently, we began testing one of the xanthene dyes, rhodamine 6G (Rh6G), on various substrates to explore the possibility of using this class of materials for gas phase sensing. To our surprise, we found that by using a three-layer system of substrate, transparent polymer and fluorophore, the emission signal could be enhanced by 2 or 3 orders of magnitude, depending on the specific structure. This makes detecting changes in the fluorescence more reliable and increases the sensitivity enormously. One of the challenges is that the interaction between the xanthenes and the analytes appears to be irreversible.

An array approach to detecting a variety of explosive analytes and related molecules is being developed. We use a three-layer structure consisting of a glass substrate, two different polymers (polymethylmethacrylate (PMMA) and polyvinylidene difluoride (PVDF)) and five different xanthene dyes. The PVDF polymers are deposited with different thickness and this changes the observed response. All of the sensors are exposed to room temperature analytes and the responses are much stronger than observed in DMF solution, with changes ranging from 100% quenching to greater than 100% enhancement of the fluorescent signal. The fluorescence difference spectrum of each of the analytes is unique, allowing identification of several common explosives, including TNT, RDX, HMX, PETN and TATP. The combined sensitivity and selectivity is unique.

D. Major Contributions

Scheme 1 on the next page shows the general structure of the three-layer sensor. A mechanical substrate, a glass slide about 1 mm thick, is spin-cast with a transparent polymer to give a layer that is a few hundred nm thick. The spin-coater was kept under a nitrogen atmosphere to reduce the humidity levels, which is known to affect the surface roughness of the polymer [39]. Then the fluorophore was spin-cast onto the polymer layer, which was a few nm thick. The structures of the dyes and polymers are also shown in Scheme 1. Two polymers were chosen, PMMA and PVDF. PVDF can form in at least three different phases and the structures of the nonpolar α-phase (where the C-C single bonds alternate between *s-trans* and *s-gauche*) and the ferroelectric β-phase (where all of the C-C bonds are *s-trans*) are shown in Scheme 1. γ-PVDF, the third common phase, is polar and the C-C chain is a sequence of three *s-trans* bonds and one *s-gauche* bond. The spin-casting method does not control the phase of the PVDF and with these very thin films, it is possible that any of the three phases are formed. Direct observation of the polymer phase by infrared (IR) spectroscopy is inconclusive because the diagnostic peaks are obscured by absorption by the glass substrate. Therefore, two thicknesses of PVDF were used; the first is very thin and might have a mixture of phases; and the other is thicker and should be primarily α-phase. The xanthene dyes have a similar chemical structure, but the charge varies: Rh6G and Rh560 are cationic; SRhB and Rh640 are zwitterionic; and Fl548 is anionic.

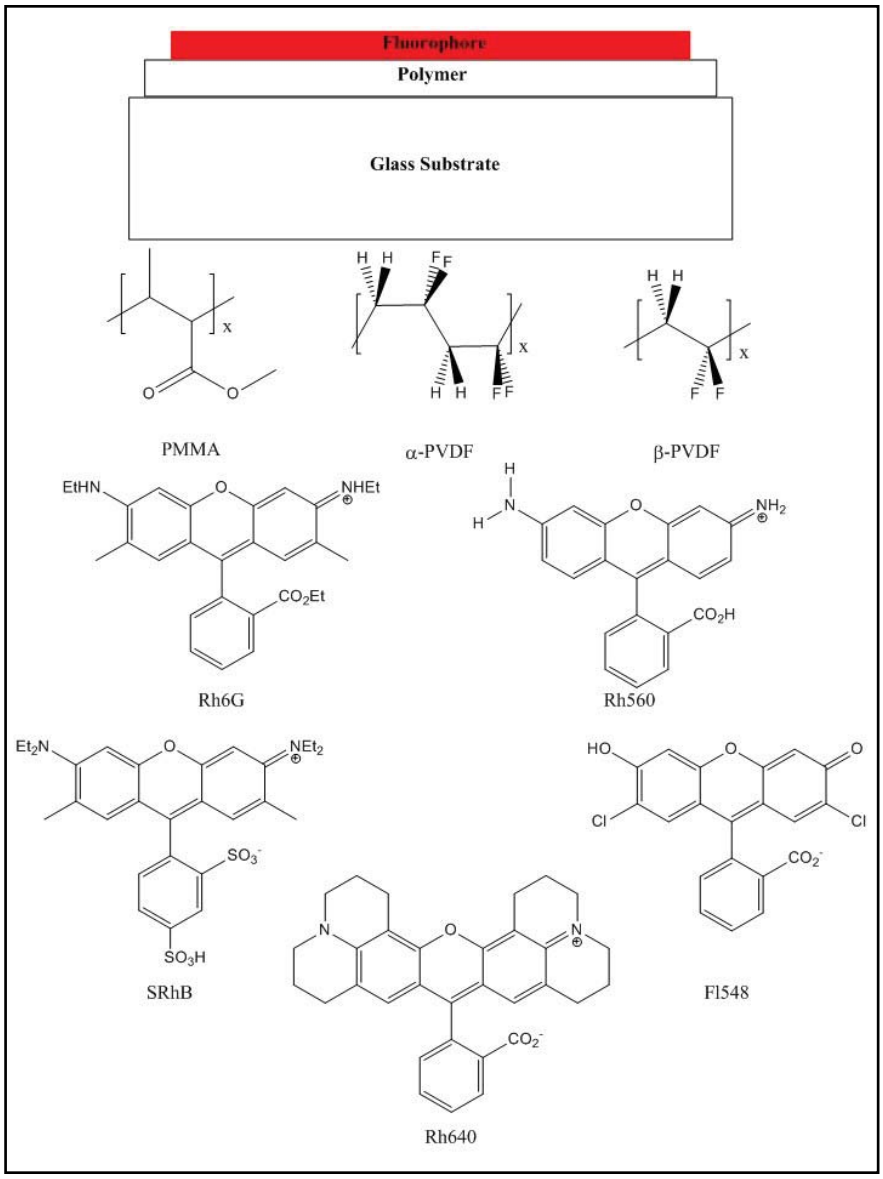

Scheme 1: General structure of the three-layer sensor.

The spectral parameters found by fitting to two Gaussian peak shapes for the various dyes are given in Table 1 on the next page. For samples with PMMA, the polymer layer was about 450 nm with a sample-to-sample variance of ±40 nm. This was measured by the fringing pattern in the absorption spectra and fitting the optical constants of the reflection spectra. For the samples with PVDF, two layer thicknesses were used: 380 nm (variance±40 nm) and 440 nm (variance ±100 nm). The PVDF samples had a strong scattering profile in the absorption spectrum and no fringing, so the thicknesses were obtained solely from the reflectance reliable spectrum. The fluorophore thicknesses could not be reliably measured but are estimated to be on the order of 1 – 10 nm thick. The lower limit of thickness measurements from the reflectance spectra are typically 10 – 20 nm and these films were thinner than that. The thickness could not be determined by AFM since a step-edge could not be formed. The baseline corrected absorbance spectra (vide infra) had absorption maxima in the 0.005 to 0.01 range. While none of the solid-state absorption coefficients are known for these chromophores, a typical estimate for a π-π* transition is 10^5 – 10^6 cm^{-1}. Thus, thicknesses in the 1 nm range are expected for these samples. For these thicknesses, the xanthene dyes are no more than 1 or 2 monolayers thick.

Sample	λ_1 (nm)	Γ_1 (nm)	a_1	λ_2 (nm)	Γ_2 (nm)	a_2
Fl548/450 nm PMMA	478 (2)	16 (3)	0.0004 (0.0001)	513 (9)	41 (4)	0.00103 (0.00002)
Fl548/380 nm PVDF	474 (2)	29 (3)	0.00199 (0.00017)	509.4 (0.4)	13.5 (0.7)	0.00152 (0.00015)
Fl548/440 nm PVDF	474 (1)	25 (1)	0.00190 (0.00007)	509.6 (0.7)	13.7 (0.5)	0.00166 (0.00011)
Rh560/450 nm PMMA	512 (5)	28 (4)	0.00481 (0.0041)			
Rh560/380 nm PVDF	504 (2)	26 (2)	0.00899 (0.00092)			
Rh560/440 nm PVDF	501.3 (0.8)	37 (1)	0.00593 (0.00018)			
Rh6G/450 nm PMMA	500 (1)	12 (2)	0.00307 (0.00053)	535.5 (0.4)	18.7 (0.6)	0.0138 (0.0004)
Rh6G/380 nm PVDF	498 (7)	26 (8)	0.0077 (0.0027)	529 (1)	20 (2)	0.0167 (0.0022)
Rh6G/440 nm PVDF	520 (2)	29 (1)	0.00891 (0.00028)	553 (1)	14 (1)	0.0029 (0.0011)
SRhB/ 450 nm PMMA	546 (4)	38 (2)	0.0183 (0.0024)	561.4 (0.4)	13 (1)	0.0145 (0.0017)
SRhB/380 nm PVDF	535 (1)	34 (1)	0.01100 (0.00034)	574 (1)	17.9 (0.5)	0.0096 (0.0011)
SRhB/440 nm PVDF	528 (9)	25 (5)	0.0083 (0.0013)	570 (4)	22 (3)	0.0143 (0.0041)
Rh640/450 nm PMMA	530 (3)	15 (3)	0.00095 (0.00024)	573.6 (0.7)	22 (1)	0.00389 (0.00030)
Rh640/380 nm PVDF	538 (4)	26 (5)	0.00146 (0.00014)	574.9 (0.8)	19.7 (0.5)	0.00370 (0.00030)
Rh640/440 nm PVDF	539 (5)	27 (10)	0.00196 (0.00068)	576 (2)	19 (1)	0.0045 (0.0020)

Table 1: Fit parameters for the absorption spectra of the five xanthene dyes on different substrates. λ_i are the absorption maxima, Γ_i are the half-width at half-height and a_i are the intensities. The values in parentheses are the standard deviations found from a minimum of 10 different samples for the indicated composition.

The fit parameters for the emission spectra are given in Table 2 on the next page. The substrate can affect either the emission intensity or the maximum peak position. Although the fluorophores are all nominally the same thickness, the intensity can vary by as much as a factor of 4 for different substrates. A significant shift of the emission maximum (~20 nm) is observed for Rh560 on PMMA compared to PVDF. Rh6G showed unusual behavior in that the emission maximum shifted not only between PMMA and PVDF substrates, but also was different for the different thicknesses of PVDF; for the thin PVDF layer (380 nm), the emission maximum was 564 nm, 15 nm higher than the maximum for the thick PVDF (440 nm), where the maximum was found at 550 nm. All of the fluorophores have a narrower high energy peak corresponding to the observed emission maximum and a wider lower energy peak.

Sample	λ_1 (nm)	Γ_1 (nm)	a_1	λ_2 (nm)	Γ_2 (nm)	a_2
Fl548/450 nm PMMA	538.1 (0.3)	14.8 (0.3)	1.5×10^5 (0.2×10^5)	558 (1)	40.6 (0.7)	1.4×10^5 (0.2×10^5)
Fl548/380 nm PVDF	533.0 (0.4)	13.1 (0.5)	2.1×10^5 (0.3×10^5)	548 (2)	38 (1)	1.5×10^5 (0.3×10^5)
Fl548/440 nm PVDF	532.7 (0.7)	12.1 (0.7)	4.1×10^4 (0.7×10^4)	539 (4)	42 (2)	4.8×10^4 (0.6×10^4)
Rh560/450 nm PMMA	528 (1)	17.9 (0.3)	1.8×10^5 (0.4×10^5)	555 (2)	34.5 (0.4)	8.1×10^4 (1.9×10^4)
Rh560/380 nm PVDF	507.9 (0.5)	17 (3)	6.4×10^5 (1.3×10^5)	517 (5)	43 (1)	7.9×10^5 (1.7×10^5)
Rh560/440 nm PVDF	507.6 (0.6)	11 (2)	7.2×10^5 (3.4×10^5)	497 (5)	55 (5)	1.3×10^5 (0.4×10^5)
Rh6G/450 nm PMMA	570.5 (0.5)	17.1 (0.2)	2.0×10^6 (0.5×10^6)	599.2 (0.8)	38.3 (0.5)	1.1×10^6 (0.3×10^6)
Rh6G/380 nm PVDF	564.0 (0.5)	29.1 (0.5)	7.0×10^6 (1.3×10^6)	588.7 (0.9)	57.6 (0.9)	3.1×10^6 (0.7×10^6)
Rh6G/440 nm PVDF	549.5 (0.8)	33.8 (0.4)	4.2×10^6 (0.2×10^6)	575 (1)	64.2 (0.5)	2.0×10^6 (0.1×10^6)
SRhB/ 450 nm PMMA	583.5 (0.3)	15.3 (0.1)	2.4×10^6 (0.4×10^6)	607.7 (0.3)	44.6 (0.3)	1.3×10^6 (0.2×10^6)
SRhB/380 nm PVDF	586.5 (0.6)	15.2 (0.2)	9.3×10^5 (3.9×10^5)	610 (1)	45.2 (0.7)	5.2×10^5 (1.6×10^5)
SRhB/440 nm PVDF	584.2 (0.6)	15.4 (0.4)	3.2×10^6 (2.5×10^6)	608 (1)	44.4 (0.8)	1.6×10^6 (1.2×10^6)
Rh640/450 nm PMMA	600.6 (0.5)	17.5 (0.1)	6.8×10^5 (1.8×10^5)	635 (2)	39 (2)	2.4×10^5 (0.6×10^5)
Rh640/380 nm PVDF	595.4 (0.8)	16.8 (0.5)	7.4×10^5 (5.9×10^5)	623 (4)	59 (10)	3.4×10^5 (3.1×10^5)
Rh640/440 nm PVDF	598 (2)	17.3 (0.2)	2.5×10^6 (3.5×10^6)	630 (4)	46 (3)	9.4×10^5 (1.4×10^6)

Table 2: Fit parameters for the emission spectra of the five xanthene dyes on different substrates. λ_i are the emission maxima, Γ_i are the half-width at half-height, and a_i are the intensities. The values in parentheses are the standard deviations found from a minimum of 10 different samples for the indicated composition.

Each of the polymer/fluorophore combinations was exposed to 11 different analytes composed of explosives or explosive-related molecules. The sensing was done at room temperature with no heating of the analyte. Exposure times varied between 10 minutes and 24 hours but no changes were observed after 10 minutes. After the exposure, the absorption and emission spectra for each sample were re-measured. Most of the emission spectra exhibited intensity changes after exposure to an analyte. The normalized emission difference spectra are shown in Figure 1 on the next page.

The majority of the emission spectra show significant intensity changes upon exposure to the analytes. The difference spectra displayed in Figure 1 on the next page show both quenching and enhancement. While previous work in DMF solution [18] suggested that these emission changes should occur, the unexpected result is that the gas phase exposure gives much larger changes than the solution phase exposure. In DMF solution, the emission changes were typically a few percent or less, except for TNT and TNB, which showed large changes because they reacted with the solvent. The results here show that the emission changes are typically

on the order of a few tens of percent. This is despite the fact that, in the solution, the relative concentration of the analyte was orders of magnitude higher than the gas phase exposures presented here. The pattern of responses across the array is unique for each analyte except 2, 3-DNT and 3, 4-DNT, which both either quench or have no response with each fluorophore/polymer combination

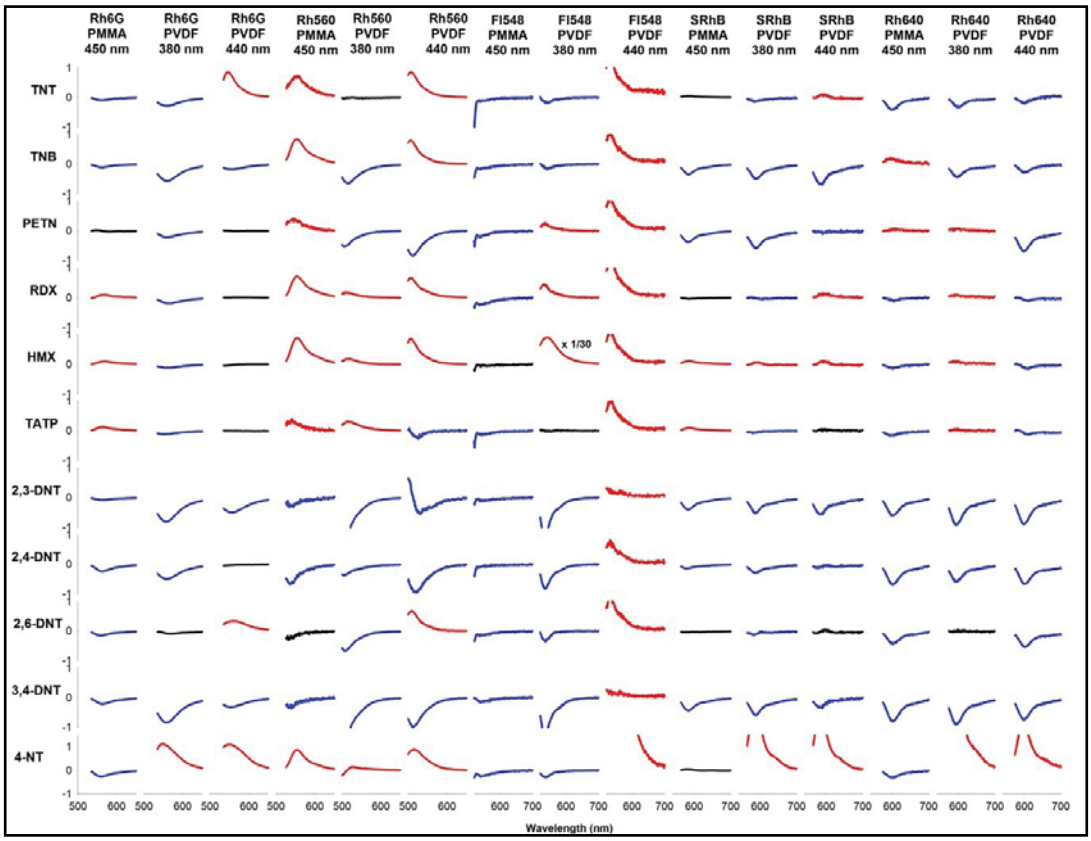

Figure 1: The emission difference spectra, showing both quenching and enhancement.

The mechanism of the fluorescence response must be an excited state interaction, at least in most cases, since the absorption spectra are generally not influenced by the presence of the analyte. Whether this excited-state interaction is through the gas phase analyte or a particulate on the surface is not known. Clearly, the nature of the interface is important; in many cases, the same fluorophore on a different polymer substrate changes the response. For example, 4-NT causes Rh6G to quench when placed on PMMA but enhances the Rh6G emission on PVDF. Even the thickness of the PVDF can cause a change in the response. For example, TNT causes quenching of Fl548 on a thin layer of PVDF but causes enhancement of Fl548 on a thicker layer of PVDF. While the causes for these observations need further study to understand, it does provide a simple method to create an array of sensors that can distinguish a large number of analytes using only a few components.

Initial investigations of the mechanism of the sensing responses were begun in Year 3. A detailed study of Rh6G on a glass substrate has revealed that the maximum fluorescence response is found from the thinnest films, as shown in Figure 2 on the next page. As the average thickness is reduced to below ~1.3 nm, the emission intensity increases dramatically. A thickness of 1 – 1.4 nm constitutes a monolayer (depending on the specific geometry of the Rh6G on the surface); so for films greater than 1.3 nm, the Rh6G is self-quenching, leading to the decreased emission. This is ideal for a sensor application. When the nominal thickness is ~0.5 nm, about 40 – 50% of the surface is covered and the emission signal is maximized. When an analyte molecule interacts with the fluorophore on the surface, the relative change in the signal is large, because a large percentage of the surface molecules are affected.

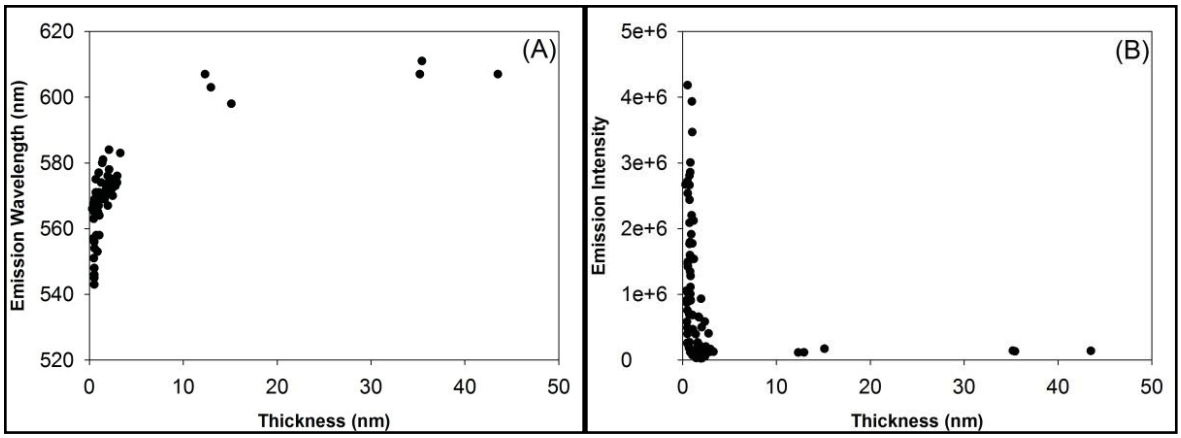

Figure 2: Emission wavelength (A) and intensity (B) as a function of Rh6G thickness.

The thicker films can also be exploited for sensing. If the film is one monolayer thick and an analyte impinges on the film, it is possible that the analyte disrupts the self-interaction between the fluorophores. If this case occurs, then the emission intensity will increase. This may explain the fluorescence enhancements observed in some cases.

The spectral results allow determination of the surface structures. The Rh6G monomer (M) is found at some concentration in all films. The absorption maximum for the monomer is 527 nm and the emission maximum is found at 550 nm and the lifetime is τ = 1.9 ns. The polarized spectra indicate that the transition moment of the monomer is located in the plane of the substrate. The second structure is an oblique dimer (D), giving rise to excitonic absorption peaks at 500 nm and 548 nm. From exciton theory [40,41], the angle θ between the transition dipoles of the two monomers can be found from the relative intensities of each absorption peak and was estimated to be $\sim 67^{o}$ ($\pm 5°$). Emission occurs from the oblique dimer only from the lower energy state, assigned to the peak at 600 nm. The third structure is an aggregate (A) (or perhaps initial crystallization) of three or more Rh6G molecules. Aggregates are only found in films with average thicknesses greater than a monolayer (>1.2 nm) and are assigned the absorption peak at 562 nm. *A* is weakly emissive at 650 nm with a lifetime of τ = 0.4 ns, typical of aggregates because of the increased number of nonradiative pathways available. Finally, the emission peak at 573 nm is assigned to an excimer (E) with a lifetime of τ = 4.0 ns. The presence of *E* is implied by the observation that the absorption and excitation spectra overlap for films less than about 1 monolayer thick, but the emission spectra show an increase in intensity in the 573 nm region as the density of molecules on the surface increases.

For the thinnest films (< 0.7 nm), the absorption is approximately equally distributed between *M* (or E) and *D*. The thinnest films prepared here, ~0.7 nm thick, are about 0.5 monolayer, assuming a closest packed structure and a spherical Rh6G with a diameter of 1.4 nm. At this thickness, only about 1.6% of the Rh6G molecules have no nearest neighbors. Thus, observation of a high percentage of *D* in the absorption is not surprising. The emission in the submonolayer films is also dominated by *M* and *E*. The lifetime of the monomer is 1.9 ns, slightly less than the 4.22 ns lifetime for Rh6G in DMF solution [18], but comprises the largest fraction of decay for films less than 0.7 nm thick. As the films become thicker, the absorption associated with *M* becomes small and that, with *A*, increases. The emission of the thicker films arises primarily from *E* and *D*. Only for the thickest films does the fraction of emission from *A* become significant, although the absolute emission is quenched.

E. Milestones

Two major objectives need to be achieved:

- Understanding the mechanism of the sensing activity.

A detailed investigation of the Rh6G on glass determined that monolayer films give the maximum signal strength in the emission spectra, which will be optimal for sensitivity. The next step is to measure the spectra when the fluorophores are placed on the polymer layers to optimize the polymer thickness and emission amplification.

- Creation and testing of an array of sensors on a single substrate.

Currently, each sensing event is done with individual sensors that are evaluated one at a time. A working system needs to be formed as an array with simultaneous detection of every pixel. This is the design criterion required for a real-time device. A chemical printer is now available for our use and we have begun printing arrays of fluorophores for initial testing in a commercial device.

F. Future Plans

The sensor platform being developed has three components: substrate, polymer and fluorophore. None of these have been optimized and each needs to be. The sensor currently consists of individually fabricated structures, and an array containing all of the pixels needs to be designed and developed. Finally, the sensing system needs to be tested in a dirty environment.

F.1. Optimization of the substrate

Our current research has used glass substrates primarily because they are inexpensive and easy to use. We know from previous research [17] that flat silicon surfaces give greater fluorescence signals but the origin of this is unknown. We also need to consider other substrates that can be used for commercialization. The sensor array will need to be printed using a chemical printer, and glass and silicon are not ideal substrates for this. Better options would be paper or light stock cardboard, so these substrates will be investigated. Our industrial partner has provided us with PVC stock to print on, and initial observations are that these work well.

F.2. Optimization of the polymer layer

A series of questions about the polymer layer need to be answered:

- What is the best thickness for the polymer layer?
- Are there more than one optimal polymer thicknesses?
- Does the polymer thickness depend on the chemical composition of the polymer? If so, how?
- Does the surface roughness of the polymer matter? If so, can we control this?
- Does the phase of the polymer matter?
- Is it better for the polymer to be crystalline or amorphous?

Spin-coating the polymer under different conditions (primarily the concentration of the polymer deposition solution or the spinning speed) allows us to control the polymer thickness to ±50 nm. The chemical composition and phase of a polymer can be determined by FTIR spectroscopy. In the case of PVDF, we can control the phase composition by the use of metal salts, which induce β-phase formation. The role of surface roughness has not been investigated previously, but this parameter can be controlled by the deposition conditions; the gas phase humidity influences the surface roughness in PVDF [39]. The surface roughness is also related to the real surface area, so the amount of fluorophore that can be deposited onto the surface can be changed, which may affect sensitivity.

F.3. Optimization of the fluorophore layer

This was accomplished in the past year. The maximum signal strength is observed when the fluorophore is approximately one monolayer thick. Determining the conditions to achieve this thickness on each substrate needs to be done.

F.4. Sensor array

Once optimum conditions for the various fluorophore/polymer combinations are determined, then a sensor array can be created. This will be done using a chemical printer that can deposit polymer or fluorophore onto a substrate at controlled locations and with controlled thicknesses. However, the deposition conditions (primarily, solution concentrations) for printing may be different than for spin-coating, so these will need to be determined. Once this is done, the pixel size for each sensing element will need to be established. The goal is to find the smallest pixel size that still gives sufficient signal-to-noise for the optical detection. As the pixel size becomes smaller, more pixels can be put onto a substrate, which gives the array better selectivity and adaptability for new analytes.

III. RELEVANCE AND TRANSITION

A. Relevance of Research to the DHS Enterprise

The objective is to create a sensor system that is: (1) sensitive enough to detect explosives at or below their natural room temperature vapor pressure; (2) selective enough to distinguish a variety of threats; (3) adaptable enough to be trained for new threats; and (4) inexpensive. The system could be developed as a handheld device for use by personnel, or as part of a passive system integrated into portals or HVAC systems.

B. Potential for Transition

Initial discussions with DetectaChem were followed up and collaboration has ensued. Samples have been provided to the company to test in their platform.

C. Transition Pathway

DetectaChem has started testing our sensing methodology in their optical platform. They have been provided with an array of fluorophores with the initial objective to determine if they can see a fluorescent signal. This will be followed up with exposure to analytes.

IV. PROJECT ACCOMPLISHMENTS AND DOCUMENTATION

A. Peer Reviewed Journal Articles

1. Hui Qi Zhang & William B. Euler. “Detection of Gas-Phase Explosive Analytes Using Fluorescent Spectroscopy of Thin Films of Xanthene Dyes.” *Sensors & Actuators B: Chemical, 225*, pp. 553-562. March 2016. DOI:10.1016/j.snb.2015.11.098
2. Mingyu Chapman, Matthew Mullen, Elsa Novoa-Ortega, Mona Alhasani, James F. Elman, & William B. Euler. “Structural Evolution of Ultrathin Films of Rhodamine 6G on Glass.” *Journal of Physical Chemistry C*, *120*(15), pp. 8289 – 8297. March 2016. DOI:10.1021/acs.jpcc.6b01669

B. Other Presentations

1. Invited Talks
   a. Euler, William B.; Zhang, Hui Qi; Liu, Mingyu; Mullen, Matthew. "Fluorescence Detection of Explosives: A Study Towards Optimization of an Array of Thin Film Optical Sensors." SciX, Providence, RI, September 28, 2015 (invited).
   b. Gupta, Anju; Conrad, Matthew; Euler, William B.; Alhasani, Mona. "Thermogravimetric Analysis (TGA) of Zinc Nitrate-Doped Polyvinylidene Fluoride Substrate for Sensor Applications." AIChE National Meeting, Salt Lake City, UT, November 12, 2015.
2. Poster Sessions
   a. Liu, Mingyu; Ortega, Elsa; Euler, William B. "Study of Rhodamine 6G Thin Films on a Glass Substrate." 250th ACS Meeting, Boston, MA, August 16, 2015.
   b. Mullen, Matthew; Alhasani, Mona; Conrad, Matthew A.; Gupta, Anju; Euler, William B. "Influence of the Interfacial Effects by PVDF on the Fluorescent Properties of Rhodamine 6G." 250th ACS Meeting, Boston, MA, August 16, 2015.

V. REFERENCES

[1] S. Yang, C. Wang, C. Liu, Y. Wang, Y. Xiao, J. Li, Y. Li, R. Yang, Anal. Chem., 2014, 86, 7931-7938. "Fluorescence Modulation by Absorbent on Solid Surface: An Improved Approach for Designing Fluorescent Sensor."

[2] J. W. Nugent, H. Lee, H.-S. Lee, J. H. Reibenspies, R. D. Hancock, Inorg. Chem., 2014, 53, 9014-9026. "The Effect of π Contacts between Metal Ions and Fluorophores on the Fluorescence of PET Sensors: Implications for Sensor Design for Cations and Anions."

[3] M. Akamatsu, T. Mori, K. Okamoto, H. Komatsu, K. Kumagai, S. Shiratori, M. Yamamura, T. Nabeshima, H. Sakai, M. Abe, J. P. Hill, K. Ariga, ACS Appl. Mater. Interfaces, 2015, 7, 6189-6194. "Detection of Ethanol in Alcoholic Beverages or Vapor Phase Using Fluorescent Molecules Embedded in a Nanofibrous Polymer."

[4] J-S. Yang and T.M. Swager, J. Am. Chem. Soc., 1998, 120, 11864-11873. "Fluorescent Porous Polymer Films as TNT Chemosensors: Electronic and Structural Effects."

[5] J-S. Yang and T.M. Swager, J. Am. Chem. Soc., 1998, 120, 5321-5322. "Porous Shape Persistent Fluorescent Polymer Films: An Approach to TNT Sensory Materials."

[6] S. J. Toal and W. C. Trogler, J. Mater. Chem., 2006, 16, 2871-2883. "Polymer Sensors for Nitroaromatic Explosives Detection."

[7] A. Levitsky, W. B. Euler, N. Tokranova, A. Rose, Appl. Phys. Lett., 2007, 90, 041904-1-041904-3. "Fluorescent Polymer - Porous Silicon Microcavity Devices for Explosives Detection."

[8] T. Naddo, Y. Che, W. Zhang, K. Balakrishnan, X. Yang, M. Yen, J. Zhao, J. S. Moore, L. Zang, J. Am. Chem. Soc., 2007, 129, 6978-6979. "Detection of Explosives with a Fluorescent Nanofibril Film"

[9] T. L. Andrew and T. M. Swager, J. Am. Chem. Soc., 2007, 129, 7254-7255. "A Fluorescence Turn-On Mechanism to Detect High Explosives RDX and PETN."

[10] J. C. Sanchez, A. G. DiPasquale, A. L. Rheingold, W. C. Trogler, Chem. Mater., 2007, 19, 6459-6470. "Synthesis, Luminescence Properties, and Explosives Sensing with 1,1-Tetraphenylsilole- and 1,1-Silafluorene-vinylene Polymers."

[11] S. W. Thomas III, G. D. Joly, T. M. Swager, Chem. Rev., 2007, 107, 1339-1386. "Chemical Sensors Based on Amplifying Fluorescent Conjugated Polymers."

[12] Q. Fang, J. Geng, B. Liu, D. Gao, F. Li, Z. Wang, G. Guan, Z. Zhang, Chem. Eur. J., 2009, 15, 11507-11514. "Inverted Opal Fluorescence Film Chemosensor for the Detection of Explosive Nitroaromatic Vapors through Fluorescence Resonance Energy Transfer."
[13] W. Chen, N. B. Zuckerman, J. P. Konopleski, S. Chen, Anal. Chem., 2010, 82, 461-465. "Pyrene-Functionalized Ruthenium Nanoparticles as Effective Chemosensors for Nitroaromatic Derivatives."
[14] R. C. Stringer, S. Gangopadhyay, S. A. Grant, Anal. Chem., 2010, 82, 4015-4019. "Pyrene-Functionalized Ruthenium Nanoparticles as Effective Chemosensors for Nitroaromatic Derivatives."
[15] Ponnu and E. V. Anslyn, Supramol. Chem., 2010, 22, 65-71. "A Fluorescence-Based Cyclodextrin Sensor to Detect Nitroaromatic Explosives."
[16] K. Zhang, H. Zhou, Q. Mei, S. Wang, G. Guan, R. Liu, J. Zhang, Z. Zhang, J. Am. Chem. Soc., 2011, 133, 8424-8427. "Instant Visual Detection of Trinitrotoluene Particulates on Various Surfaces by Ratiometric Fluorescence of Dual-Emission Quantum Dots Hybrid."
[17] M. A. Matoian, R. Sweetman, E. C. Hall, S. Albanese, W. B. Euler, J. Fluoresc., 2013, 23, 877-880. "Light Trapping to Amplify Metal Enhanced Fluorescence with Application for TNT Sensing."
[18] A. Latendresse, S.C. Fernandes, S. You, H. Q. Zhang, W. B. Euler, Anal. Methods, 2013, 5, 5457-5463. "A Fluorometric Array for the Detection of Military Explosives and IED Materials."
[19] K. Liu, T. Liu, X. Chen, X. Sun, Y. Fang, ACS Appl. Mater. Interfaces, 2013, 5, 9830-9836. "Fluorescent Films Based on Molecular-Gel Networks and Their Sensing Performances."
[20] P. Sabherwal, M. Shorie, P. Pathania, S. Chaudhary, K. K. Bhasin, V. Bhalla, C. R. Suri, Anal. Chem., 2014, 86, 7200-7204. "Hybrid Aptamer-Antibody Linked Fluorescence Resonance Energy Transfer Based Detection of Trinitrotoluene."
[21] Dinda, A. Gupta, B. K. Shaw, S. Sadhu, S. K. Saha, ACS Appl. Mater. Interfaces, 2014, 6, 10722-10728. "Highly Selective Detection of Trinitrophenol by Luminescent Functionalized Reduced Graphene Oxide through FRET Mechanism."
[22] Y.-N. Gong, Y.-L. Huang, L. Jiang, T.-B. Lu, Inorg. Chem., 2014, 53, 9457-9459. "A Luminescent Microporous Metal−Organic Framework with Highly Selective CO_2 Adsorption and Sensing of Nitro Explosives."
[23] Y. Wang and Y. Ni, Anal. Chem., 2014, 86, 7463-7470. "Molybdenum Disulfide Quantum Dots as a Photoluminescence Sensing Platform for 2,4,6-Trinitrophenol Detection."
[24] H. Chen and Y. Xia, Anal. Chem., 2014, 86, 11062-11069. "Compact Hybrid (Gold Nanodendrite-Quantum Dots) Assembly: Plasmon Enhanced Fluorescence-Based Platform for Small Molecule Sensing in Solution."
[25] L. Ding, Y. Bai, Y. Cao, G. Ren, G. J. Blanchard, Y. Fang, Langmuir, 2014, 30, 7645-7653. "Micelle-Induced Versatile Sensing Behavior of Bispyrene-Based Fluorescent Molecular Sensor for Picric Acid and PYX Explosives."
[26] M. Bai, S. Huang, S. Xu, G. Hu, L. Wang, Anal. Chem., 2015, 87, 2383-2388. "Fluorescent Nanosensors via Photoinduced Polymerization of Hydrophobic Inorganic Quantum Dots for the Sensitive and Selective Detection of Nitroaromatics."
[27] M. Rong, L. Lin, X. Song, T. Zhao, Y. Zhong, J. Yan, Y. Wang, X. Chen, Anal. Chem., 2015, 87, 1288-1296. "A Label-Free Fluorescence Sensing Approach for Selective and Sensitive Detection of 2,4,6-Trinitrophenol (TNP) in Aqueous Solution Using Graphitic Carbon Nitride Nanosheets."
[28] L. Zhang, Y. Han, J. Zhu, Y. Zhai, S. Dong, Anal. Chem., 2015, 87, 2033-2036. "Simple and Sensitive Fluorescent and Electrochemical Trinitrotoluene Sensors Based on Aqueous Carbon Dots."
[29] Wade, P. Lovera, D. O'Carroll, H. Doyle, G. Redmond, Anal. Chem., 2015, 87, 4421-4428. "Luminescent Optical Detection of Volatile Electron Deficient Compounds by Conjugated Polymer Nano-

fibers."

[30] F.-N. Xiao, K. Wang, F.-B. Wang, X.-H. Xia, Anal. Chem., 2015, 87, 4530-4537. "Highly Stable and Luminescent Layered Hybrid Materials for Sensitive Detection of TNT Explosives."

[31] N. Venkatramaiah, C. F. Pereira, R. F. Mendes, F. A. A. Paz, J. P. C. Tomé, Anal. Chem., 2015, 87, 4515-4522. "Phosphonate Appended Porphyrins as Versatile Chemosensors for Selective Detection of Trinitrotoluene."

[32] J. Ma, L. Lv, G. Zou, Q. Zhang, ACS Appl. Mater. Interfaces, 2015, 7, 241-249. "Fluorescent Porous Film Modified Polymer Optical Fiber via "Click" Chemistry: Stable Dye Dispersion and Trace Explosive Detection."

[33] W. Xie, S.-R. Zhang, D.-Y. Du, J.-S. Qin, S.-J. Bao, J. Li, Z.-M. Su, W.-W. He, Q. Fu, Y.-Q. Lan, Inorg. Chem., 2015, 54, 3290-3296. "Stable Luminescent Metal−Organic Frameworks as Dual-Functional Materials to Encapsulate Ln^{3+} Ions for White-Light Emission and To Detect Nitroaromatic Explosives."

[34] P. Joo, K. Jo, G. Ahn, D. Voiry, H. Y. Jeong, S. Ryu, M. Chhowalla, B.-S. Kim, Nano Lett., 2014, 14, 6456-6462. "Functional Polyelectrolyte Nanospaced MoS_2 Multilayers for Enhanced Photoluminescence."

[35] W. Chen, Q. Li, W. Zheng, F. Hu, G. Zhang, Z. Wang, D. Zhang, X. Jiang, Angew. Chem.Int. Ed., 2014, 53, 13734-13739. "Identification of Bacteria in Water by a Fluorescent Arrray."

[36] W. Xu, C. Ren, C. L. Teoh, J. Peng, S. H. Gadre, H.-W. Rhee, C.-L. K. Lee, Y.-T. Chang, Anal. Chem., 2014, 86, 8763-8769. "An Artificial Tongue Fluorescent Sensor Array for Identification and Quantitation of Various Heavy Metal Ions."

[37] S. Wang, L. Ding, J. Fan, Z. Wang, Y. Fang, ACS Appl. Mater. Interfaces, 2014, 6, 16156-16165. "Bispyrene/Surfactant-Assembly-Based Fluorescent Sensor Array for Discriminating Lanthanide Ions in Aqueous Solution."

[38] Y. Wu, Y. Tan, J. Wu, S. Chen, Y. Z. Chen, X. Zhou, Y. Jiang, C. Tan, ACS Appl. Mater. Interfaces, 2015, 7, 6882-6888. "Fluorescence Array-Based Sensing of Metal Ions Using Conjugated Polyelectrolytes."

[39] M. Benz, W. B. Euler, O. J. Gregory, Langmuir, 2001, 17, 239-243. "The Influence of Preparation Conditions on the Surface Morphology of Poly(vinylidenefluoride) Films."

[40] M. Kasha, H. R. Rawls, M. Ashraf El-Bayoumi, Pure Appl. Chem., 1965, 11, 371–392. "The Exciton Model in Molecular Spectroscopy."

[41] M. Kasha, Radiat. Res., 1963, 20, 55–70. "Energy Transfer Mechanisms and the Molecular Exciton Model for Molecular Aggregates."